

Journal of Materials Chemistry A

Ultra-Low Ice Adhesion Enabled by Nano-Engineered Poly (ionic liquid)-Elastomeric Films: Leveraging Aqueous Lubrication and Elasticity

Journal:	Journal of Materials Chemistry A
Manuscript ID	TA-ART-07-2024-004704.R1
Article Type:	Paper
Date Submitted by the Author:	01-Sep-2024
Complete List of Authors:	Mossayebi, Zahra; The University of Melbourne Faculty of Engineering and Information Technology, Chemical and Biomolecular Engineering; CSIRO Manufacturing and Materials Technology, Gurr, Paul; The University of Melbourne, Chemical and Biomolecular Engineering Simons, Ranya; CSIRO, CMSE Qiao, Greg; The University of Melbourne, Chemical and Biomolecular Engineering

SCHOLARONE™ Manuscripts

ARTICLE

Received 00th January 20xx, Accepted 00th January 20xx

DOI: 10.1039/x0xx000000x

Ultra-Low Ice Adhesion Enabled by Nano-Engineered Poly (ionic liquid)-Elastomeric Films: Leveraging Aqueous Lubrication and Elasticity

Zahra Mossayebi, ab Paul A. Gurr, Ranya Simons*b and Greg G. Qiao*a

Ice accumulation poses challenges across diverse industries. For effective passive ice removal, surfaces must achieve ultralow ice adhesion strength (τ_{ice}), ideally below 10 kPa. Such low ice adhesion values with persistent functionality are rarely reported. Typically, coatings exhibited such qualities require increased thicknesses, often ranging in the hundreds of microns, thereby compromising scalability. This study introduces novel poly (ionic liquid) (PIL)-based elastomeric thin films, nano-engineered through a unique surface-initiated polymerization technique called solid-state continuous assembly of polymers (ssCAP), incorporating a new amphiphilic PIL-based lubricant (AmL). Nano-scale surface-confined polydimethylsiloxane networks with enhanced elasticity and chain mobility achieved by precisely controlling the crosslinking density. Addition of 20 wt% AmL to a highly elastic, surface-tethered network imparted a thin PIL-infused film with ultra-low ice adhesion strength $\tau_{ice} \sim 1.4$ kPa, showcasing a one-order-of-magnitude reduction in τ_{ice} . Leveraging elasticity and interfacial aqueous lubrication have led to this passive ice shedding, making this the first instance of such a low value in hydrated coatings. This thin PIL-elastomeric film retained its ice adhesion strength below 10 kPa even after tape peeling, prolonged water exposure, and 15 icing/de-icing cycles. This is likely attributed to the robust ssCAP_{ROMP} chemistry and rationally designed amphiphilic lubricant ensuring its effective integration within the elastomeric network. Remarkably, the film developed here is only 30 nm thick, obviating the need for the considerable thickness typically required by other soft coatings. This work aims to establish design guidelines for the next generation of thin icephobic coatings, harnessing synergistic design strategies and robust surface chemistries.

Introduction

Unwanted ice build-up can lead to serious damage and safety hazards for aircraft, power lines, wind turbines and marine structures. The two main strategies for addressing ice accretion involve active methods, such as post-formation heating, and passive approaches, such as protective anti-icing coatings, with a growing preference for passive methods due to their cost-effectiveness and lower environmental impact. To qualify as anti-icing, a surface must resist ice formation and/or adhesion, with a primary focus on minimizing ice adhesion, given the inevitability of ice formation, particularly in harsh subzero environments. Le can easily fall off surfaces that have ultra-low ice adhesion strength $\tau_{\rm ice} < 10~{\rm kPa}$ under gravitational forces or natural airflow. Recently, the threshold of ice adhesion strength has been minimized to below 10 kPa through a

Ice detachment on elastomeric surfaces arises from the considerable mismatch in the elastic modulus (E) between the ice and elastomer, resulting in deformation incompatibility under stress and facilitated ice removal.^{5,11} Golovin et al.^{12,13} investigated the impact of two main contributors on the viscoelastic nature and, ultimately, ice adhesion of elastomeric surfaces: crosslinking density and interfacial slippage. Adjusting the crosslinking density could effectively modify the physical stiffness and elastic modulus of elastomers, achieving ultra-low τ_{ice} solely by significant reduction in the degrees of crosslinking. Moreover, enhancing the chain mobility of elastomers through the incorporation of miscible polymers into them endowed the so-called interfacial slippage (IS) mechanism, resulting in remarkably low ice adhesion strength (τ_{ice} = 3.6 ± 1.0 kPa). Importantly, interfacial slippage differs from the lubrication mechanism observed on surfaces with a lubricant top-layer. 13,14 When crosslinked polymeric matrices, commonly Sylgard 184, are infused with various organic liquids like silicon oil/paraffin,^{15–21} short/long-chain alkanes,^{22,23} Krytox,¹³ etc., organogels are created. Depending on the viscosity and concentration of the oil,13,23 a slippery interface with a continuous lubricating layer forms between the organogel and

transition from conventional micro/nano structures to surfaces with controlled physicochemical properties, such as elasticity and lubricity. $^{6-10}$

a. Department of Chemical Engineering, The University of Melbourne, Melbourne, Victoria 3010, Australia.

b. CSIRO manufacturing, Melbourne, Victoria 3196, Australia.

[†]Electronic Supplementary Information (ESI) available: Supporting figures and tables for Results and Discussion, Fig. S1-S6, Table S1-S3. See DOI: 10.1039/x0xx00000x.

ice, resulting in exceptional anti-icing performance ($\tau_{ice} \leq 1$ kPa). 13,22,24 Cohesive failure, deriving from the sacrificial nature (i.e., loss) of the lubricant, is the primary contributor to the low ice adhesion strength in this class of organogels, leading to their poor durability. $^{25-27}$ Recently, several strategies have improved the retention of lubricant in self-lubricating organogels (SLUGs) through the autonomous generation of the interfacial lubricant layer upon ice contact, achieved by leveraging the syneresis effect or depressing the freezing point of water. 22,28 However, this self-lubricating capability is typically restricted to several cycles of icing and de-icing.

Other groups have utilized the synergy of various icephobic mechanisms within the same coating to achieve ultra-low ice adhesion strength.5,29 Reducing the elastic modulus and facilitating interfacial slippage simultaneously, or integrating a low elastic modulus with a lubricating interface, are viable strategies to minimize elastic deformation and/or the work of adhesion, resulting in easier ice detachment. 13,14,24,30 While cutting-edge organogels and low elastic modulus surfaces significantly decrease ice adhesion strength, challenges such as poor mechanical robustness, lubricant depletion, and weak substrate adhesion continue to compromise their long-term effectiveness. Importantly, the enhanced resistance to ice adhesion in these coatings depends on a substantial increased thickness ranging in the hundreds of microns, 13,14 which is typically not scalable. Therefore, the creation of ultra-slippery elastomers with exceptional ice adhesion resistance and enhanced stability calls for innovative nano-scale surfaceconfined chemistries and anti-icing lubricants, eliminating the dependence on increased thickness.

Herein, we present a novel approach utilizing solid-state continuous assembly of polymers (ssCAP) to design ultra-thin poly(ionic liquid) (PIL)-based elastomeric films with super-low ice adhesion, thereby enabling the synergistic effects of aqueous lubrication and interfacial slippage. The ssCAP technique, recently developed in our group,31-33 offers a notable advantage over existing crosslinking methods in the literature. It enabled simultaneous crosslinking and directional growth of the elastomers from the substrate at nano-scale, ensuring adjustable elasticity while providing covalent surface confinement. Therefore, the key approaches of this study were as follows: 1) as the first instance of utilizing ssCAP for anti-icing low-elastic modulus polydimethylsiloxane (PDMS)-based thin films formed in a controlled manner, yet strongly adhered to the substrate; 2) introduction of a new amphiphilic lubricant into elastomers, instead of traditional hydrophobic lubricant. The triblock amphiphilic lubricant designed to immobilize the poly (ionic liquid) (PIL) anti-freezing groups into a PDMS backbone to improve not only the affinity of the lubricant to the PDMS elastomeric network but also the retention of the functional components; 3) for the first time, the integration of an amphiphilic lubricant into a surfacebound/low-crosslinked elastomer utilizes both the anti-icing mechanisms of interfacial slippage and aqueous lubrication to

achieve lower ice adhesion strength. Inclusion of amphiphilic lubricant contributes not only to the generation of a water lubricating layer and ultra-slippery interface but also promotes chain mobility to induce interfacial slippage in chemically grafted elastomers; 4) the newly developed coatings do not need to be significantly thick to achieve ultra-low ice adhesion strength, unlike soft hydrophobic organogels. 13,14 Only a thickness of 30 nm is sufficient to yield an ultra-low shear stress; and finally, 5) improved stability in the surface-confined poly (ionic liquid) (PIL)-based elastomer, attributed not only to the robust surface chemistry of ssCAP but also the amphiphilic nature of the lubricant. This leads us to the critical research question: "Can nano-engineered elastomeric coatings achieve ice adhesion strength below 10 kPa?" We envision that our innovative nanotechnology and design strategy will establish guidelines for outstanding and long-lasting anti-icing capabilities.

Results and discussion

Synthesis of Macrocrosslinkers and surface-tethered Elastomers/PIL-infused Elastomers via ssCAP_{ROMP} Procedure. The ssCAP, a solid-state surface-initiated polymerization technique, utilizes polymer macrocrosslinkers containing polymerizable norbornene (NB) pendants form crosslinked/surface-tethered films through a controlled polymerization process known as ring-opening metathesis polymerization (ROMP), referred to as ssCAP_{ROMP}. A newly designed PDMS-based macrocrosslinker has been specifically tailored for this innovative approach, facilitating the production of surface-bound thin elastomers with precisely controlled thickness and crosslinking density. PIL-infused elastomers were subsequently created by introducing an amphiphilic PIL-based lubricant into the elastomers via $\mathsf{ssCAP}_{\mathsf{ROMP}}$ procedure. Therefore, we designed: 1) crosslinked nano-coatings that are covalently bound to the surface, and 2) a unique amphiphilic lubricant that effectively 'locks' into the coating. The lubricant comprises a hydrophobic backbone to increase compatibility with the network and hydrophilic PIL pendants to interact with ice.

To synthesize the macrocrosslinkers, a PDMS-based macroinitiator was prepared according to our previous work34 and then polymerized via reversible addition–fragmentation chain transfer (RAFT) polymerization to incorporate highly reactive pendent NB moieties, as depicted in Fig. 1a. By controlling the feed ratios of monomer (M), the content of crosslinkable NB groups in the resulting triblock copolymers of PDMS-b-(PNBMMA)₂ was adjusted to 5 mol% (P5) and 10 mol% (P10), as confirmed by 1H NMR and gel permeation chromatography (GPC) analysis (Supporting Information Fig. S1 and Table S1). To further reduce the crosslinking density of our elastomers, we synthesized a norbornene-terminated PDMS macrocrosslinker (NB-PDMS-NB, P2) through the esterification reaction between exo-5-norbornenecarboxylic acid and a

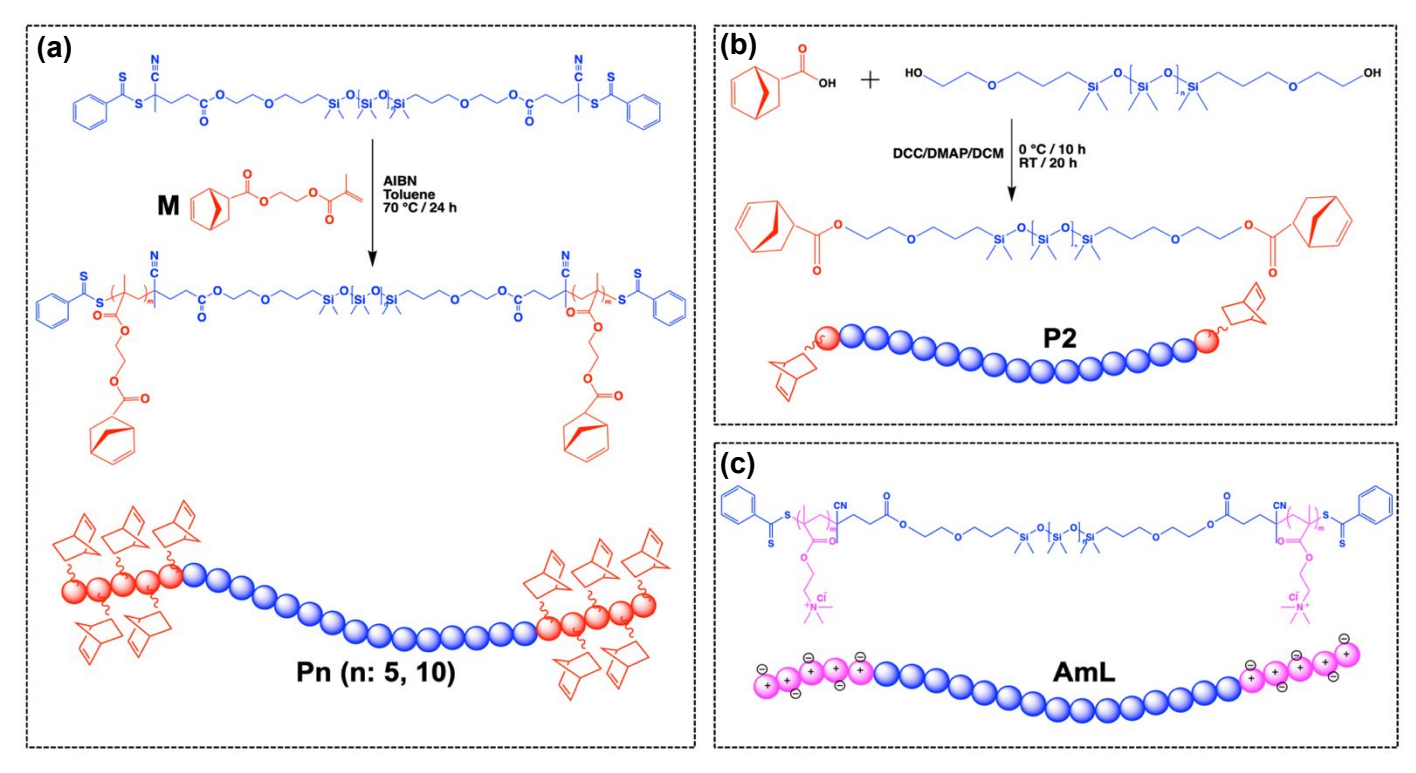


Fig. 1 Chemical schematic of the synthesized macrocrosslinkers and amphiphilic lubricant: (a) Triblock copolymers of PDMS-b-(PNBMMA)₂ containing 5 mol% (P5) and 10 mol% (P10) norbornene moieties, (b) Norbornene-terminated PDMS (NB-PDMS-NB, P2) and, (c) Poly(ionic liquid)-based amphiphilic lubricant (AmL) which is a triblock copolymer of PDMS-b-(PMETAC)₂.

commercially available bis-(hydroxyethyloxypropyl) polydimethylsiloxane, as illustrated in Fig. 1b and characterized in Supporting Information Figure S2. Additionally, the amphiphilic lubricant, a triblock copolymer of PDMS-b-(PMETAC)₂, was obtained via RAFT polymerization of PDMS-based macroinitiator and 2-(methacryloyloxy)ethyl trimethylammonium chloride (METAC), as described in our previous study.³⁴ The resulting amphiphilic lubricant, denoted as AmL and presented in Fig. 1c, contained approximately 11 mol% of the PIL component.

To facilitate surface-initiated crosslinking via $\mathsf{ssCAP}_{\mathsf{ROMP}}$, we implemented several pre-modification steps following a previously established procedure, 31-33 as depicted in Fig. 2. Initially, we allyl-functionalized plasma-treated substrates by immersing them in a solution of allyl-modified poly(ethylene imine) (allyl-PEI) (Fig. 2a), followed by immobilization of the Grubbs Generation III catalyst onto the allyl-terminated surfaces to create initiation sites for the ROMP reaction (Figure 2b). Unlike other controlled/surface-initiated polymerization methods that require oxygen-free environments and external stimuli for film growth or crosslinking, 35,36 our ssCAP_{ROMP} method allows for simultaneous directional growth/crosslinking and film formation under ambient conditions, owing to the oxygen tolerance of the Grubbs Generation III catalyst^{37,38} and the low glass transition temperature of our designed macrocrosslinkers. Subsequently, spin-coating a solution of macrocrosslinkers on the catalyzed substrates allowed crosslinking of the films via surface-initiated ROMP at room temperature. After 24 h of reaction, the

polymerization was terminated using a solution of ethyl vinyl ether, followed by thorough rinsing to remove non-crosslinked polymers and form surface-grafted thin elastomers (Fig. 2c). Depending on the content of the pendant NB groups in the macrocrosslinkers (Pn, n: 2, 5, 10), the resultant elastomeric films with varied degrees of crosslinking (En, n: 2, 5, 10, i.e. E2, E5 and E10 respectively) were expected to exhibit different behaviours under stress. Independently, upon spin-coating a macrocrosslinker solution with added amphiphilic lubricant (20 and 50 wt.% of AmL) onto the catalyzed substrates and subjecting them to the same ssCAP_{ROMP} procedure (Fig. 2d), surface-confined PIL-infused elastomers formed, designated as En-Lm, where "m" represents the AmL loading (0, 20 and 50 wt.%, i.e. L0, L20 and L50 respectively). It should be noted that En-L0 refers to the plain PDMS elastomeric films and is same as

Adopting the ssCAP_{ROMP} strategy and introducing crosslinkable NB species into a PDMS-based macrocrosslinker, elastomers (En) were produced with strong substrate bonding and tuneable elasticity in a precisely controlled manner. The versatility of this approach and the rational design of the amphiphilic lubricant allows for adequate locking of the lubricant into the elastomeric network. The resulting PIL-infused elastomers (En-Lm) adhered well to the substrate, combining the flexibility of the PDMS network with the lipophilicity³⁰ of the PDMS backbone in the lubricant, while also featuring a continuous self-lubricating interface under icing conditions due to PIL segments of the lubricant.³⁴ Therefore, we designed: 1) crosslinked nanocoatings which are covalently bonded to the surface, and 2)

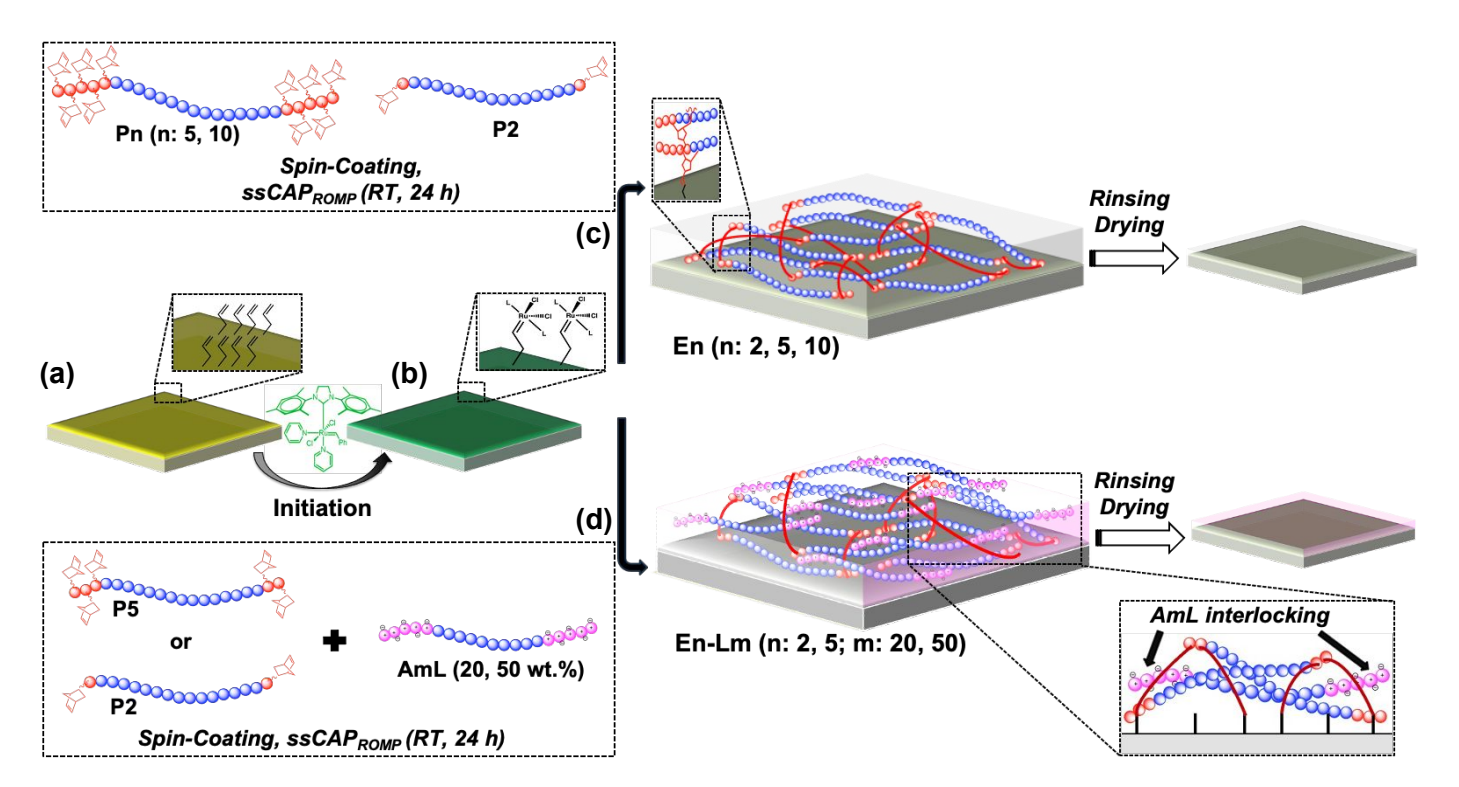


Fig. 2 Schematic illustration of ssCAP_{ROMP} procedure for fabrication of surface-tethered/crosslinked thin films: (a) functionalization of the substrate with allyl-PEI, (b) immobilization of metathesis catalyst (i.e., initiation layer), formation of (c) elastomers, and (d) Poly (ionic liquid) (PIL)-infused elastomers.

unique amphiphilic lubricant that effectively 'locks' into the coating, comprising hydrophobic backbone to increase compatibility with the network and hydrophilic PIL pendants to interact with ice.

Film Growth and Surface Characterization of Elastomers and PIL-infused Elastomers. The growth of crosslinked films mediated by surface-initiated ROMP is depicted in Fig. 3a. The thickness was determined by measuring the step-height of a scratched film using atomic force microscopy (AFM)³⁹ (Supporting Information Fig. S3a). Ranging from 35 nm to 239 nm, a rapid growth rate was observed for En elastomers with increasing NB content (i.e. n), as expected. Depending on the lubricant uptake, embedding AmL into elastomers slightly increased the thickness of PIL-infused elastomers, in particular E5-L20 and E5-L50. This is likely due to their swollen/less-crosslinked networks compared to those pristine elastomers with the same NB content, indicating relatively different growth kinetics and crosslinking density for lubricant-contained elastomers.

Film roughness was consistent and relatively low ($R_q \le 4$ nm) in surface-tethered En elastomers (Fig. 3b and Supporting Information Fig. S3b), suggesting that polymer crosslinks are evenly formed across the planar surface. Furthermore, we did not observe any distinct AmL lubricating layer in the AFM images of our PIL-infused elastomers, similar to those oil-infused networks with interfacial slippage reported elsewhere. This observation sets our PIL-infused elastomers apart from the lubricated organogels, in which the added oil phase separates from the elastomeric matrices and generates a

lubricating oil top layer that is readily visible in optical/AFM images.

X-ray photoelectron spectroscopy (XPS) analysis was performed on En elastomers (with E5 as a representative) and compared to a freshly plasma-cleaned silicon substrate. The representative sample E5 is shown in the Supporting Information Fig. S4 with a summary of the results tabulated in Table S2. Relative to a cleaned silicon wafer substrate, the C 1s spectrum of the E5 elastomer revealed appearance of an intense C 1s peak, predominantly featuring a C–Si signal around 284.3 eV. Furthermore, the Si 2p spectrum of the E5 elastomer exhibited the disappearance of a set of doublet peaks centred at around 103 eV, corresponding to the native silicon oxide layer of the substrate, and instead revealed a notable contribution of siloxane bonds (i.e., $-O-Si(CH3)_2-O-$) around 102 eV.^{40,41} These observations indicate the successful assembly of Pn polymers on the surface via ssCAP_{ROMP}.

In the case of PIL-infused elastomers, the presence of PIL domains within the PDMS network was investigated using EDX elemental mapping (Supporting Information Fig. S5). The uniform distribution of chlorine, representing the PIL segments of the amphiphilic lubricant, supports the successful embedment of the lubricant into the elastomeric matrices while it was absent in the E2 coating.

Ice Adhesion Reduction in Elastomers and PIL-infused Elastomers. As a key measure of surface icephobicity, ice adhesion strength values are determined by applying force (F) to detach adhered ice with a specific contact area (A) from the surface. Initially, we used a custom-built apparatus, as per our

Journal of Materials Chemistry A

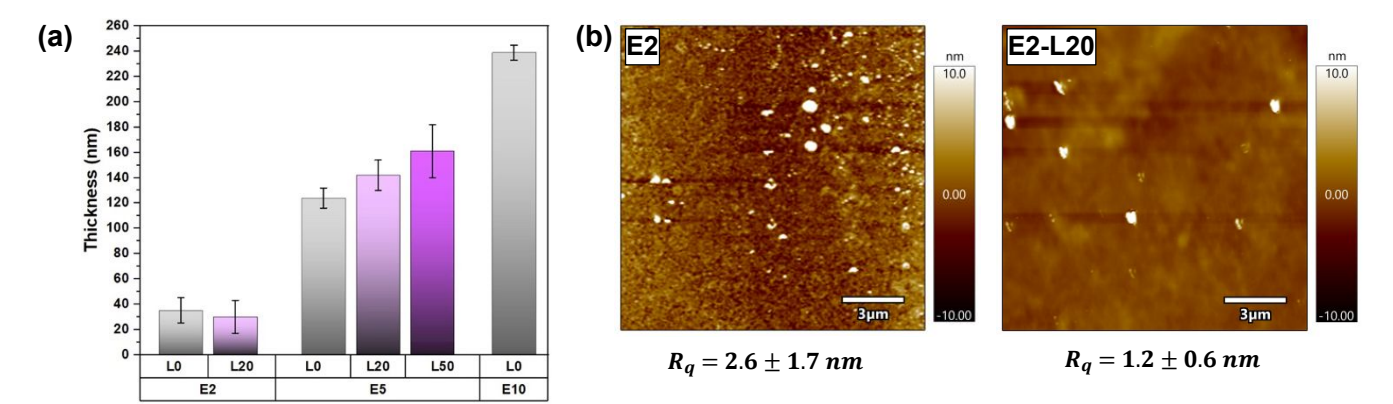


Fig. 3 Characterization of the fabricated elastomers and PIL-infused elastomers using ssCAP_{ROMP} procedure: (a) films' growth and thickness after 24 h reaction, estimated by AFM scratch technique, (b) topography and roughness of the films represented in AFM height images.

prior research, 34 to measure ice adhesion strength in the tensile mode (σ_{ice} , kPa). However, for measurements below ultra-low adhesion levels (<10 kPa), which was under the detection limit of the apparatus, a new setup was utilized to determine adhesion strength in the shear mode (τ_{ice} , kPa), using a cooling stage, force transducer and syringe pump (see Materials and Methods).

In Fig. 4a, three En elastomers with varying NB crosslinkable pendant content were tested to explore the influence of crosslinking density on the tensile detachment of ice from surface-bound films. Previous literature suggests a strong correlation between the physical stiffness, elastic modulus of PDMS elastomers, and the degree of crosslinking. 13,14 Less crosslinked networks are believed to facilitate ice removal due to a greater mismatch in elastic modulus between the ice and siloxane elastomer.^{5,30} Similarly, the chemically grafted films here exhibited a remarkable reduction in ice adhesion solely through decreasing crosslinking density. A nearly twofold reduction in adhesion strength was observed for the E5 coating (σ_{ice} = 69.4 ± 6.2 kPa) compared to E10 (σ_{ice} = 143.6 ± 23.4 kPa), indicating a direct correlation between crosslinking density and tensile ice adhesion in films of equal thickness. Additionally, we determined further reduction in ice adhesion for the lesscrosslinked E2 film (σ_{ice} = 26.7 ± 6 kPa).

We tried to deepen our understanding of this relationship by utilizing AFM Force Spectroscopy to measure the elastic modulus of En elastomers. However, this measurement was challenging due to the ultra-thin nature of the surface-confined films, 19 and thus, precise values could not be obtained. Moreover, we found no significant difference in the advancing (θ_{adv}) and receding (θ_{rec}) contact angles of the En elastomers (Supporting Information Table S3) suggesting that variations observed in σ_{ice} were primarily influenced by changes in crosslinking density rather than the work of adhesion, which is related to the parameter (1+cos θ_{rec}). 11,13,14,42 Hence, our findings imply that the mobility of polymeric chains in En films is altered by their degree of crosslinking, despite being chemically bound to the substrate. This alteration potentially leads to a lower elastic modulus and, consequently, reduced ice adhesion strength in the E2 coating.

As illustrated in Fig. 4b, the infusion of PIL-based amphiphilic lubricant (AmL) into elastomeric matrices results in a substantial decrease in ice adhesion strength in PIL-infused elastomers (En-Lm), approaching a value of σ_{ice} ~13.3 kPa. This value corresponds to a control sample, an aluminium substrate spincoated with just AmL lubricant, denoted as AmL at 100 wt.% on the X-axis. The measured ice adhesion strengths for the E5-L20 and E5-L50 coatings were 41.6 \pm 5.5 kPa and 32.1 \pm 7.4 kPa, respectively. The ice adhesion reduction in En-Lm coatings is attributed to the creation of an aqueous lubricating layer at the interface upon contact with ice, effectively transforming its state from solid to slippery. A phenomenon proved in our previous research indicating that the interaction between water molecules and PIL components of AmL promotes the formation of a thin hydration layer at the interface, acting as a selflubricating layer that diminishes ice adhesion strength on the surface.34 Furthermore, the observed decrease in ice adhesion in En-Lm films can also be attributed to a potential reduction in crosslinking density and, consequently, the elastic modulus with increasing lubricant content. The addition of uncrosslinked polymeric chains of AmL to the solution of macrocrosslinkers (Pn) leads to less-crosslinked networks in En-Lm films compared to En, owing to their steric hindrance effect during ssCAP_{ROMP} reaction, and consequently resulting in a lower elastic modulus. It is important to note that the AmL contents, presented in Fig. 4b and 4c are theoretical values, which may not precisely reflect the actual intake of lubricant because the ssCAP_{ROMP} reaction was terminated after 24 hours and unreacted precursors were thoroughly rinsed off the surface. Hence, complete diffusion of the lubricant into the networks cannot be guaranteed making it difficult to measure the actual intake.

As can be seen in Fig. 4b, the ice adhesion strength of the E2-L20 film fell below the detection limit of the apparatus in tensile mode (σ_{ice} < 10 kPa). Therefore, the critical shear force required to remove ice from such surfaces was measured using a setup in shear mode at -10 °C, and the ice adhesion strength (τ_{ice}) results are represented in Figure 4c. Incorporation of 20 wt% AmL into the low-crosslinked E2 network endowed a film with an ultra-low ice adhesion strength (τ_{ice} ~1.4 kPa), in contrast to τ_{ice} ~15.8 kPa for the E2 network, thus meeting the criterion for

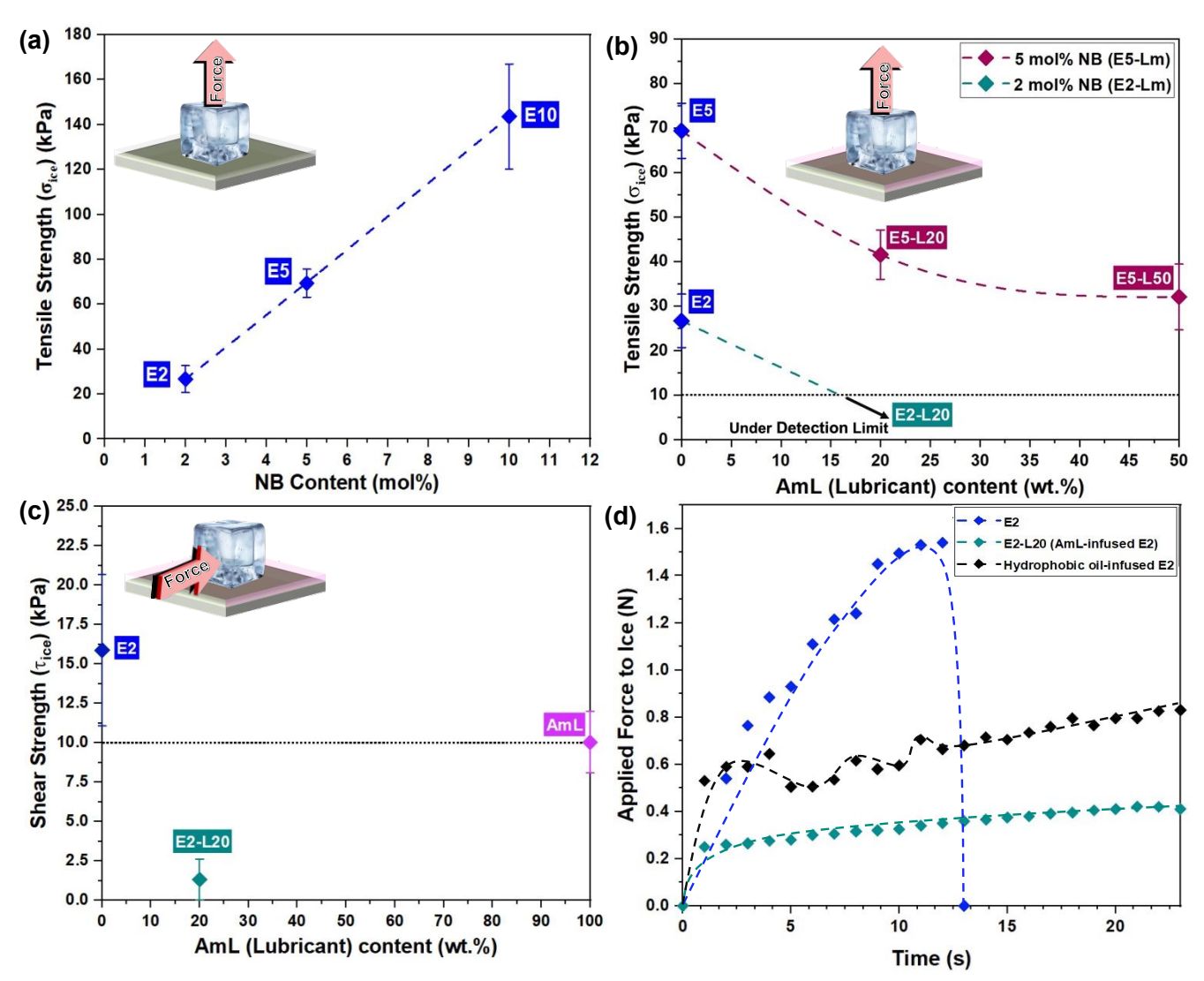


Fig. 4 Ice adhesion reduction in elastomers (En) and PIL-infused Elastomers (En-Lm): (a) effect of crosslinking density (i.e., content of crosslinkable norbornene (NB) pendants) on the tensile detachment of ice from surface-bound En, (b) variations in the tensile ice adhesion reduction in En-Lm surfaces with the amount of infiltrated amphiphilic lubricant (AmL). Noted that the tensile strength for the E2-L20 sample is below the detection limit of the apparatus, (c) shear ice adhesion strength in E2, E2-L20 and the control coating (AmL) fabricated by spin-coating AmL lubricant onto aluminium substrate. (d) force—time curves derived from the shear ice detachment. The hydrophobic oil-infused E2 is a control coating prepared by substituting the amphiphilic lubricant (AmL) with a hydrophobic PDMS-based lubricant of identical structure to AmL but lacking PIL segments. Note: AmL contents, presented here, are theoretical values and not necessarily the actual intake. Additionally, the dashed lines in the graphs represent potential trends.

passive ice removal by natural forces.⁵ According to literature, the stress needed to shear ice from a soft film, such as an elastomeric coating, is correlated with the elastic modulus E, work of adhesion (Wadh), and thickness of the film. 11,43 The inclusion of AmL into E2 is expected to not only reduce E, as previously hypothesized, but also Wadh (Supporting Information Table S3, see changes in θ_{rec}). With both films being equally thick, the synergy between E and W_{adh} effectively contributed to this one order of magnitude reduction in τ_{ice} in E2-L20 compared to the plain E2 elastomer. Consequently, the integration of amphiphilic lubricant into the surfacebound/low-crosslinked elastomer with intrinsic deformability enhanced the effectiveness of each mechanism, significantly reducing ice adhesion through the dual anti-icing mechanisms of elastic deformation and aqueous lubrication.

The force—time curves derived from shear ice detachment were analyzed to elucidate anti-icing mechanisms (Fig. 4d). On the surface-confined/crosslinked E2 elastomer, the applied force increased rapidly until reaching the critical shear stress, resulting in ice detachment from the surface, followed by an abrupt drop. This type of ice removal, termed as "sticky", is typically ascribed to the interfacial cavitation mechanism in soft elastomers. 13,43–45

To gain a comprehensive mechanistic understanding of antiicing in the amphiphilic lubricant (AmL) containing E2-L20 film, we prepared a control film of hydrophobic oil-infused E2 by substituting the amphiphilic lubricant (AmL) with a hydrophobic PDMS-based lubricant of identical structure to AmL but lacking PIL segments. This control coating, referred to as hydrophobic oil-infused E2 in Figure 4d, was fabricated to serve as a comparative reference to assess the significance of the PIL components in E2-L20 for reducing ice adhesion. In contrast to the E2 elastomer, this control coating exhibited a so-called "stick-slip" behavior during ice removal, rather than experiencing instantaneous detachment. When the critical shear stress was reached, the ice began to slide across the surface, displaying fluctuations in friction force until it was completely pushed off. This observation aligns with the dynamic stick-slip motion reported for PDMS organogels by Beemer et al.¹⁴ In their organogels, the absence of residual lubricant on ice post-separation suggested that no lubricant layer formed at the interface. Similarly, no oil microdroplets were observed on ice after removal from our hydrophobic oil-infused E2. Consequently, we hypothesize that the stick-slip friction characteristic arises from either enhanced chain mobility and elasticity due to lubricant addition and/or the presence of a non-uniform interfacial oil layer, which facilitates localized ice detachment and sliding. Here, the introduction of lubricant is believed to lead to a less-crosslinked network, consequently inducing a degree of interfacial slippage that reduces the strength of ice adhesion. However, confirming its synergism with localized lubrication remains challenging.

In our observations, neither of the "sticky" nor "stick-slip" antiicing behaviors were evident in the E2-L20 coating (Fig. 4c). Instead, once the maximum applied force was overcome and ice detached, it simply slid across the surface, displaying only a "slip" characteristic during removal. The incorporation of AmL into E2 facilitated this slippage of ice under a persistent frictional force following its detachment. This resulted in a nonzero force regime in E2-L20, contrasting with E2, where the force immediately dropped to zero upon ice detachment. We also observed not only a more slippery interface during ice removal on the E2-L20 coating, but also a significant reduction in ice adhesion ($\tau_{\rm ice} \simeq 1.4$ kPa) compared to the control coating, hydrophobic oil-infused E2, which had an ice adhesion strength of about 6.5 kPa. These observations further support our hypothesis that, like the control coating, the introduction of AmL contributed to enhanced chain mobility, consequently diminishing ice adhesion strength through interfacial slippage. However, unlike the control coating, which exhibited stick-slip motion and localized lubrication, the creation of a uniform self-lubricating water layer at the interface rendered E2-L20 exceptionally slippery, significantly improving its anti-icing efficacy.

Based on our prior research findings,³⁴ we discovered that poly(ionic liquid) groups located at both ends of AmL, ionized in contact with water/ice, depressing the freezing point of water and generating a quasi-liquid lubricating layer at the interface. The active ionic groups presented on the surface of E2-L20 disrupt the original hydrogen-bonding network in water molecules through electrostatic interactions, resulting in an ultra-slippery interface through this "ion-induced icing delay"⁴⁶ phenomenon. To investigate electrostatic properties at the surface of En-Lm films, we conducted surface potential microscopy (i.e., Kelvin probe force microscopy (KPFM)) via AFM.

Our observations revealed that E2-L20 exhibited distribution of charge across its surface, with a mean value of surface potential around 531.8 ± 7.2 mV, comparable to that of the AmL coating

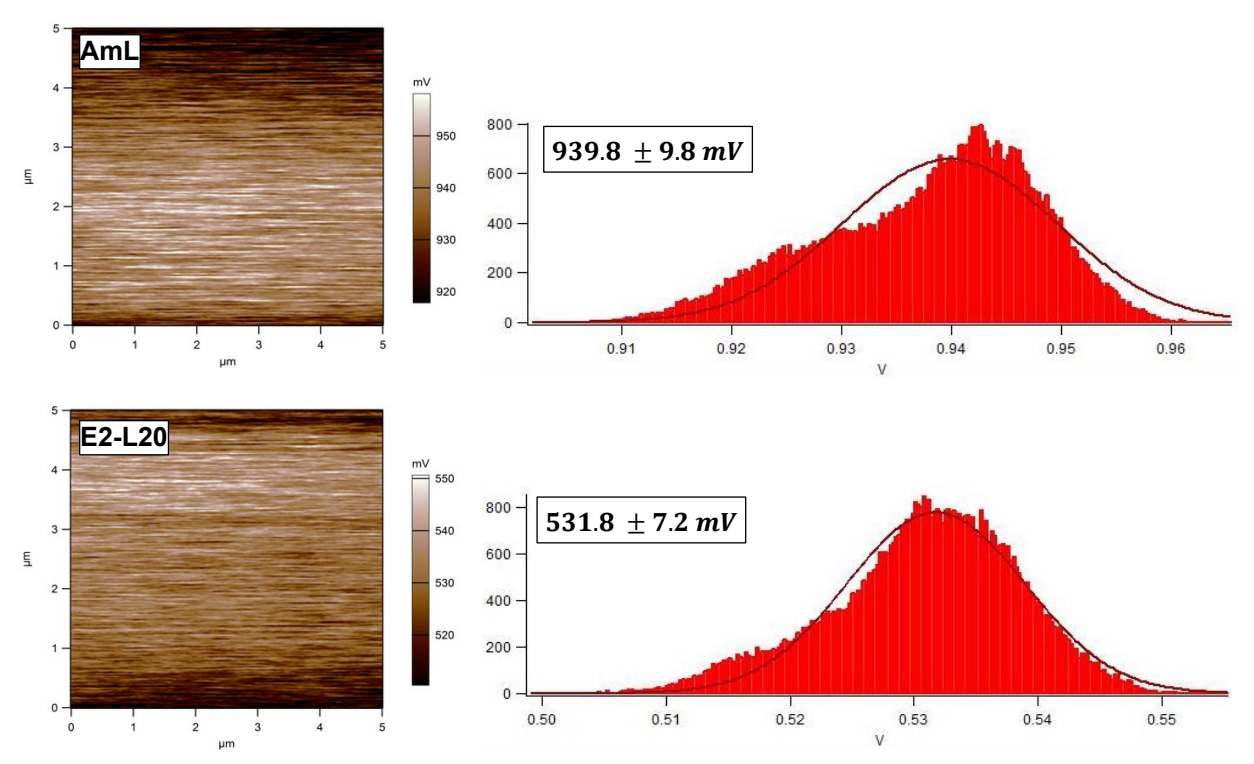


Fig. 5 Surface potential measurements on the surface of AmL control coating and PIL-infused film (E2-L20) using Kelvin probe force microscopy (KPFM). This includes statistical histograms and Gauss function fitting results of the images to obtain mean values of the contact potential difference (CPD).

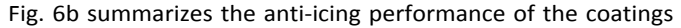
(Fig. 5). This underscores the significant role of aqueous lubrication as an anti-icing mechanism in PIL-infused films, with the presence of PIL groups confirmed on their surfaces by surface potential microscopy. Consequently, by harnessing the synergistic effects of aqueous lubrication and interfacial slippage in E2-L20 film, we achieved an ultra-slippery elastomer with super-low ice adhesion strength ($\tau_{ice} \simeq 1.4$ kPa). It is worth noting that further investigation is necessary to determine the individual contribution of each mechanism, a task that poses significant challenges.

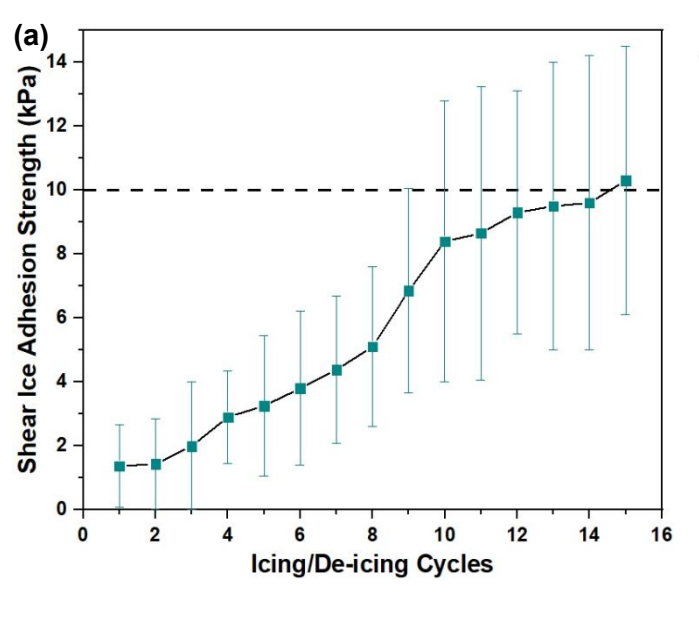
Stability of anti-icing performance and mechanical robustness of E2-L20 coating. We carried out a series of durability tests on our best-performing anti-icing coating (i.e., E2-L20). The mechanical strength was assessed through the pencil hardness (ASTM D3363) and crosshatch (ASTM D3359-09^{£2}) tests utilizing Field Emission Scanning Electron Microscopy (FESEM) to precisely detect any potential damage on the surface of nanoscale films. As depicted in Fig. S6a (Supporting Information), no discernible damage was observed along the crosshatched lines of the E2-L20 film, indicating a 5B rating for the adhesion of the film to the aluminium substrate. Although the lubricant-infused coatings are often prone to delamination due to the presence of free oil within their structure, 8,10,27 our surface-confined/crosslinked E2-L20 film, fabricated via ssCAP_{ROMP} procedure, exhibited strong adhesion to the substrate through covalent bonding. We additionally categorized the E2-L20 film as a soft coating (~ 3B) based on the hardness measurements (Supporting Information Fig. S6b).

Moreover, we investigated the persistence of anti-icing capabilities in E2-L20 coating following tape peeling, prolonged water exposure, and rigorous icing/de-icing cycles. Fig. 6a illustrates the results of ice adhesion strength throughout repeated icing/de-icing tests. While a gradual increase in τ_{ice}

value was observed with the increase of cycles, E2-L20 maintained its ice adhesion strength below an ultra-low threshold (τ_{ice} < 10 kPa) even after 15 icing/de-icing tests, ensuring passive ice removal. We attribute this reduction to the formation of mechanical scratches induced by this cyclic process. The inherent softness of the coating renders it susceptible to damage from mechanical friction. Nonetheless, it remains comparable to the few reported coatings in the literature that have sustained ice adhesion strength below 10 kPa for multiple cycles, albeit with thicknesses ranging in the hundreds of microns. $^{13,14,18,22-24,47}$

A frequent issue with lubricated organogels is the gradual depletion of the hydrophobic lubricant. However, for our coating (E2-L20), the ice adhesion strength remained nearly constant even after subjecting it to a 24-hour water immersion or peeling off a pressure-sensitive tape (3M Scotch 600) from the surface at a 180° angle (see Fig. 6b). This indicates that the amphiphilic lubricant is effectively trapped within the crosslinked/surface-confined PDMS matrices, likely due to robust ssCAP_{ROMP} chemistry and a strong affinity between the long hydrophobic backbone of the AmL lubricant and the PDMS network. This retention capability could ensure a long-lasting ultra-slippery interface in E2-L20 when in contact with ice. Furthermore, in our previous study,34 our AmL-based coating exhibited excellent anti-dehydration properties, and the interfacial aqueous layer could continuously replenish, by absorbing water molecules from the Consequently, our amphiphilic lubricant shows great promise for the development of stable lubricant-infused coatings compared to hydrophobic lubricants, as self-lubrication is an inherent feature of these systems rather than relying on external sources of lubrication.





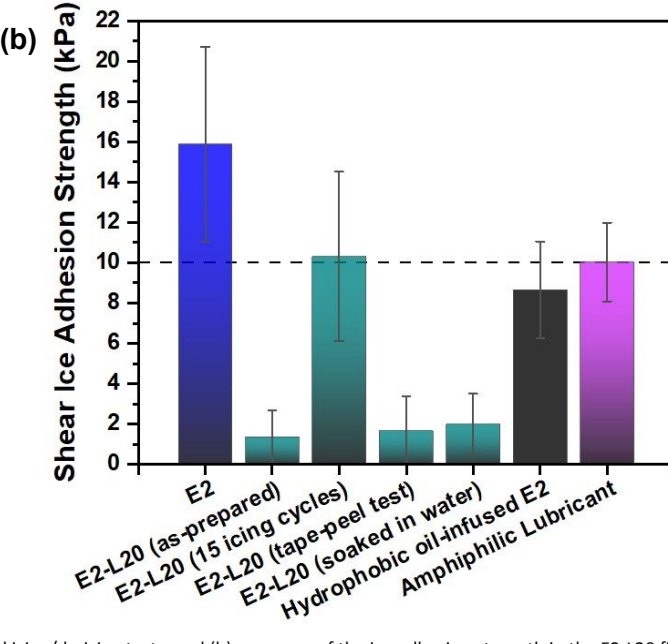


Figure 6. (a) the ice adhesion strength of the PIL-infused film of E2-L20 over repeated icing/de-icing tests, and (b) summary of the ice adhesion strength in the E2-L20 film compared to other control coatings, both before and after the stability tests.

developed in this study including the control hydrophobic oilinfused coating and stability results. Overall, the incorporation of our newly designed amphiphilic lubricant into a surface-bound/low-crosslinked elastomer using novel ssCAP_ROMP chemistry has significantly reduced the threshold of ice adhesion strength in hydrated coatings to ultra-low values ($\tau_{ice} \simeq 1.4 \ kPa$) for the first time, a feat achieved by only a few state-of-the-art coatings such as organogels and stress-localization. 13,22,24,47

Conclusions

The In conclusion, we have introduced a new controlled coating fabrication process called solid-state continuous assembly of polymers (ssCAP) via ring-opening metathesis polymerization (ROMP), referred to as ssCAP_{ROMP}, for fabricating nano-scale anti-icing surfaces. By employing this approach and incorporating crosslinkable species into a PDMS pre-polymer (specified as macrocrosslinker), we obtained thin surfacetethered elastomers (En) with precisely adjustable elasticity. The versatility of ssCAP_{ROMP}, along with a rationally designed amphiphilic lubricant (PIL-PDMS-PIL, a triblock copolymer with a central hydrophobic PDMS block and hydrophilic poly(ionic liquid) (PIL) segments at both ends), ensures effective locking of the lubricant within the elastomeric network. The resulting surface-confined PIL-infused elastomers (En-Lm) exhibited both flexibility and an aqueous self-lubricating interface under icing conditions, leading to an ultra-low ice adhesion strength (τ_{ice} \sim 1.4 kPa) in a nano-scale film containing only 20 wt% of the lubricant (E2-L20). The generation of aqueous lubrication as one of the anti-icing mechanisms in E2-L20 is confirmed by the presence of PIL groups on its surface, as revealed by surface potential microscopy. However, determining the precise contribution of each mechanism remains challenging. Future research will thoroughly explore the potential of these coatings to delay droplet freezing. Our ultra-thin surface-confined and crosslinked E2-L20 film demonstrated strong adhesion to the substrate via covalent bonding, confirmed by the crosshatch test. It also maintained its ice adhesion strength below an ultralow threshold (τ_{ice} < 10 kPa) even after 15 icing/de-icing tests, ensuring persistent anti-icing functionality. However, further reduction in adhesion strength may be attributed to the inherent softness of the coating, making it susceptible to mechanical scratches during this cyclic process. Importantly, E2-L20 retained its ultra-low ice adhesion strength even after tape peeling and prolonged water exposure, indicating effective locking of the amphiphilic lubricant into its structure. Thus, the novel nano-engineered PIL-elastomeric film presented in this study shows promising potential for anti-icing applications, offering a significant reduction in the threshold of ice adhesion strength in hydrated coatings to ultra-low values for the first time. At only 30 nm in thickness, the film developed here eliminates the need for substantial thick layers often found in other soft coatings. Improved icing/de-icing cycles can be achieved by readily incorporating thicker films through successive multilayers via ssCAP. This study provides valuable

insights for designing next generation thin icephobic coatings with passive ice removal capability.

Materials and Methods

Materials. Allyl bromide (90%), 2'-azobis-(isobutyronitrile) (AIBN), 4cyanopentanoic acid dithiobenzoate (CPADB), dimethylaminopyridine (DMAP, ≥99%), ethyl vinyl ether (EVE, 99%), exo-5-norbornenecarboxylic acid (98%), Grubbs Catalyst® M204 (2nd Generation), 2-hydroxyethyl methacrylate (HEMA, ≥99%),[2-(methacryloyloxy)ethyl]trimethylammonium chloride (METAC, 80 wt.% in H2O), N,N'-dicyclohexylcarbodiimide (DCC, 99%), poly(ethylene imine) (PEI) (Mw ~ 25 kDa), triethylamine (TEA, ≥99%) were all purchased from Sigma-Aldrich and used as received. Bis(hydroxyethyloxypropyl) polydimethylsiloxane (HO-PDMS-OH, DMS-C21, 110-140 cSt) was supplied by Gelest. Anhydrous, deoxygenated dichloromethane (DCM) prepared by vacuum distillation. Chloroform, ethanol, methanol, n-hexane, pentane, toluene, and all other solvents were obtained from Merck. Pyridine from Scharlau was used for modification of Grubbs Catalyst® M204 (2nd Generation) to 3rd generation, according to the literature.⁴⁸ Hyperbranched poly (N-allyl ethylene imine) (allyl-PEI) and 2-(methacryloyloxy)ethyl bicyclo[2.2.1]hept-5-ene-2-carboxylate (norbornene-based monomer (M)) were prepared following the procedures described elsewhere.32,49 Silicon wafer (type P) and aluminium panel (aircraft grade 2024-T3, 50 × 50 mm2, 1 mm thick) were purchased from ProSciTech and a local supplier by CSIRO manufacturing, respectively.

Characterization. Proton (1H) Nuclear Magnetic Resonance (NMR) spectroscopy was done using an Agilent 500 MHz spectrometer and CDCl₃ as reference and solvent. Gel Permeation Chromatography (GPC) analysis was performed on a Shimadzu system. The GPC columns were calibrated with low dispersity polystyrene (PSt) standards, THF was used as the eluent and an ASTRA 8.1.0 software analysed the raw data. The norbornene-based monomer (M) was purified on a fully automated Pure FlashPrep Chromatography System (BUCHI, C-850) integrated with UV-Vis and ELS detectors, fitted with a prepacked silica flash column (24g). X-ray photoelectron spectroscopy (XPS) analysis was performed using an AXIS Nova spectrometer (Kratos Analytical Inc., Manchester, UK) with a monochromated Al Kα source operating at 180W (15 kV Å~ 12mA) and a hemispherical analyzer in the fixed analyzer transmission mode. Each specimen was analyzed at an emission angle of 0° and data processing was carried out using CASAXPS processing software (Casa Software Ltd., Teignmouth, UK). A Hitachi FlexSEM 1000 microscope was employed for Scanning electron microscopy (SEM) and Energy-dispersive X-ray (EDX) elemental mappings. Atomic force microscopy (AFM) and Kelvin probe force microscopy (KPFM) were employed to acquire height and surface potential images, utilizing an Asylum Research Cypher machine equipped with Cypher software for image processing. Additionally, film thicknesses were estimated via AFM through scratching the surface and analysing the profile of the scratched zone. The static and dynamic contact angles of the deposited 5 µL water droplet on the surface were recorded on a Dataphysics OCA 20 tensiometer and the data were analysed via SCA20 software. To evaluate the mechanical strength of the films, the crosshatch test (ASTM D3359-09ε2) and pencil hardness test **ARTICLE**

(ASTM D3363) were conducted following the procedure detailed in our prior research. 34

The ice adhesion strength of thin films in tensile mode was measured using an Instron Universal Testing Machine within an environmental chamber at -20 °C, as described in our previous study. 34 Additionally, a custom-built apparatus, comprising a Peltier plate, a force transducer (Starr Instrument, model FGD-50), and a syringe pump, was established to determine the critical shear force. Icephobic coatings were pre-cooled on the Peltier plate at -10 °C. Subsequently, a square acrylic cuvette with a surface area of 1 cm2 was placed on the coatings and filled with deionized water (1 mL). The assembly was then left to freeze for 1 hour inside a chamber purged with N2 gas to prevent frost formation. The force was applied to the side of the ice column at a constant rate of 50 μm s-1, controlled by the syringe pump, until reaching the critical shear stress, at which point the ice detached from the surface. A 4 mm diameter probe of the force transducer was used, with its center precisely positioned 3 mm above the surface of the coatings. Considering that the ice adhesion on elastomers is influenced by the applied shear rate, we regulated our shear rate to remain below the upper limit of the critical shear rate (0.1 mm s-1) for the measurement of ice adhesion.⁴⁷ The reported value is the average of 10 measurements taken from different replicates.

Synthesis of Macrocrosslinkers (Pn). For the synthesis of P5 and P10 macrocrosslinkers, the PDMS-based RAFT macroinitiator (1.3 g, 0.1 mmol), norbornene-based monomer (M, (0.13 g, 0.5 mmol for P5), and (0.25 g, 1.0 mmol, for P10)), and AIBN were dissolved in toluene and deoxygenated with argon gas for 30 mins at room temperature. Subsequently, the sealed flask was allowed to stir for 24 hours at 70 °C and then cooled down to room temperature to terminate the RAFT polymerization reaction. The resultant triblock copolymers of PDMS-b-(PNBMMA) $_2$ (i.e., P5 and P10) were obtained by precipitating the reaction mixture in acetone (3 times) and vacuum-drying at 45 °C overnight.

In a separate procedure, to synthesize the norbornene-terminated PDMS macrocrosslinker (NB-PDMS-NB, i.e. P2), OH-PDMS-OH (13.0 g, 1.0 mmol), DCC (0.7 g, 4.5 mmol) exo-5-norbornenecarboxylic acid (0.55 g, 4.0 mmol), and DMAP (0.1 g, 0.9 mmol) were dissolved in anhydrous DCM (30 mL) and stirred for 24 h under nitrogen at room temperature. The reaction mixture was then filtered and subsequently concentrated under reduced pressure. The crude product was washed with methanol at least five times until all the impurities were completely removed. The obtained product was then fully dried to yield a transparent viscous liquid (8.5 g, 64.2 % yield). $^1\mathrm{H}$ NMR (500 MHz, CDCl3): δ 6.2-6.09 (m, 3H), 5.95-5.93 (m, 1H), 4.26 (m, 4H), 3.65 (t, 4H), 3.44 (m, 4H), 3.03 (s, 1H), 2.91 (s, 1H), 2.29-2.26 (m, 1H), 1.9 (m, 1H), 1.55 (m, 4H), 1.51-1.49 (m, 1H), 1.39-1.34 (m, 2H), 0.55 (m, 4H), 0-0.2 (m, (6n + 12)H) ppm.

Fabrication of surface-tethered Elastomers (En) and PIL-infused Elastomers (En-Lm) via ssCAP_{ROMP} Procedure. A silicon wafer (1 cm x 1 cm) was cleaned by sonicating in acetone and plasma-treated for 45 min using a UV/Ozone ProCleanerTM Plus unit (BIOFORCE NANOSCIENCE, Model No. UV.TC.220). It was then immediately immersed in an allyl-PEI solution being passed through a 0.45 μm filter (1 mL, 2.5 mg mL-1 in 0.5 M NaCl buffer). After an hour, it was removed from the solution and washed several times with water, THF and DCM, respectively. Next, it was transferred into a pre-dried

vial purged with argon and exposed to a solution of Grubbs Generation III catalyst (1 mL, 1 mM). After standing at room temperature for 45 min and subsequent rinsing with DCM and drying under vacuum, a solution of Pn macrocrosslinker (100 µL, 100 mg mL⁻ 1) was deposited onto the catalysed surface. The ssCAPROMP reaction was allowed to run for 24 h under ambient conditions and terminated by subjecting it to a solution of ethyl vinyl ether (2% v/v in DCM) for 1 hour. The polymer-coated surface was then washed with DCM and chloroform and subsequently soaked in chloroform for 12 hours to remove any non-crosslinked and physiosorbed polymers. After drying under vacuum, surface-confined thin elastomers (En) were used for further surface characterization tests. For anti-icing characterizations, the above procedure was applied to aluminium substrates (5 cm x 5 cm) using solutions with five-times increased volume. Independently, to create surface-confined PILinfused elastomers (En-Lm), we followed the same ssCAPROMP procedure by spin-coating a solution containing Pn and amphiphilic lubricant (20 and 50 wt.% of AmL, 100 mg mL⁻¹ in chloroform) onto catalysed surfaces. The rest of the steps remained the same as described above.

Conflicts of interest

There are no conflicts to declare.

Data availability

The data supporting this article have been included as part of the Supplementary Information.

Acknowledgements

The authors would like to express their gratitude to Daniel J Eyckens for his support with dynamic contact angle measurements, as well as to the Materials Characterisation and Fabrication Platform (MCFP) at the University of Melbourne, particularly to Tian Zheng. ZM is supported by the University of Melbourne Graduate Research Scholarship and the CSIRO-University of Melbourne student agreement.

Notes and references

- P. Irajizad, S. Nazifi, and H. Ghasemi, Advances in Colloid and Interface Science, 2019, 269, 203–218.
- 2 L. B. Boinovich, and A. M. Emelyanenko, *Advances in Colloid and Interface Science*, 2024, **323**, 103057.
- 3 H. Sojoudi, M. Wang, N. D. Boscher, G. H. McKinley, and K. K. Gleason, *Soft Matter*, 2016, **12 (7)**, 1938–1963.
- 4 M. J. Kreder, J. Alvarenga, P. Kim, and J. Aizenberg, *Nat Rev Mater*, 2016, **1** (1), 15003.
- 5 Y. Zhuo, S. Xiao, A. Amirfazli, J. He, and Z. Zhang, *Chemical Engineering Journal*, 2021, **405**, 127088.
- 6 S. Yang, C. Wu, G. Zhao, J. Sun, X. Yao, X. Ma, and Z. Wang, Cell Reports Physical Science, 2021, 2 (7), 100474.
- 7 F. Wang, Y. Zhuo, Z. He, S. Xiao, J. He, and Z. Zhang, *Advanced Science*, 2021, **8 (21)**, 2101163.
- 8 Y. Zhuo, J. Chen, S. Xiao, T. Li, F. Wang, J. He, and Z. Zhang, Mater. Horiz., 2021, 8 (12), 3266–3280.

Journal of Materials Chemistry A

- 9 M. Shamshiri, R. Jafari, and G. Momen, *Surface and Coatings Technology*, 2021, **424**, 127656.
- 10 L. Zeng, X. Lin, P. Li, F.-Q. Liu, H. Guo, and W.-H. Li, *Progress in Organic Coatings*, 2021, **159**, 106417.
- 11 M. K. Chaudhury, and K. H. Kim, Eur. Phys. J. E, 2007, 23 (2), 175–183.
- 12 K. Golovin, and A. Tuteja, Sci. Adv., 2017, 3 (9), e1701617.
- 13 K. Golovin, S. P. R. Kobaku, D. H. Lee, E. T. DiLoreto, J. M. Mabry, and A. Tuteja, *Sci. Adv.*, 2016, **2 (3)**, e1501496.
- 14 D. L. Beemer, W. Wang, and A. K. Kota, *J. Mater. Chem. A*, 2016, **4 (47)**, 18253–18258.
- 15 P. F. Ibáñez-Ibáñez, F. J. Montes Ruiz-Cabello, M. A. Cabrerizo-Vílchez, and M. A. Rodríguez-Valverde, *Journal of Colloid and Interface Science*, 2022, **608**, 792–799.
- 16 H. Qi, X. Lei, J. Gu, Y. Zhang, X. Gu, G. Zhao, and J. Yu, *Progress in Organic Coatings*, 2023, **177**, 107435.
- 17 S. Gao, B. Liu, J. Peng, K. Zhu, Y. Zhao, X. Li, and X. Yuan, ACS Appl. Mater. Interfaces, 2019, 11 (4), 4654–4666.
- 18 Y. Wang, X. Yao, J. Chen, Z. He, J. Liu, Q. Li, J. Wang, and L. Jiang, *Sci. China Mater.*, 2015, **58 (7)**, 559–565.
- 19 H. Zheng, G. Liu, B. B. Nienhaus, J. V. Buddingh, ACS Appl. Mater. Interfaces, 2022, 14 (4), 6071–6082.
- 20 Y. H. Yeong, A. Milionis, E. Loth, J. Sokhey, *Cold Regions Science and Technology*, 2018, **148**, 29–37.
- 21 X. Yao, J. Ju, S. Yang, J. Wang, and L. Jiang, *Advanced Materials*, 2014, **26 (12)**, 1895–1900.
- 22 C. Urata, G. J. Dunderdale, M. W. England, and A. Hozumi, *J. Mater. Chem. A*, 2015, **3 (24)**, 12626–12630.
- 23 C. Urata, H. Nagashima, B. D. Hatton, and A. Hozumi, ACS Appl. Mater. Interfaces, 2021, 13 (24), 28925–28937.
- 24 Y. Ru, R. Fang, Z. Gu, L. Jiang, and M. Liu, *Angewandte Chemie*, 2020, **132 (29)**, 11974–11978.
- 2020, 132 (23), 11974–11976.
 25 S. B. Subramanyam, K. Rykaczewski, and K. K. Varanasi, *Langmuir*, 2013, 29 (44), 13414–13418.
- 26 J.-H. Kim, and J. P. Rothstein, *Exp Fluids*, 2016, **57 (5)**, 81.
- 27 A. Nistal, B. Sierra-Martín, and A. Fernández-Barbero, *Materials*, 2023, **17 (1)**, 235.
- 28 Y. Yu, B. Jin, M. I. Jamil, D. Cheng, Q. Zhang, X. Zhan, and F. Chen, ACS Appl. Mater. Interfaces, 2019, 11 (13), 12838–12845.
- 29 Y. Shen, X. Wu, J. Tao, C. Zhu, Y. Lai, and Z. Chen, *Progress in Materials Science*, 2019, **103**, 509–557.
- 30 Z. Wang, Z. Zhao, G. Wen, Y. Zhu, J. Chen, X. Jing, S. Sun, L. Zhang, X. Liu, and H. Chen, ACS Nano, 2023, 17 (14), 13724–13733.
- 31 E. Nam, J. Kim, S. N. Guntari, H. Seyler, Q. Fu, E. H. H. Wong, A. Blencowe, D. J. Jones, F. Caruso, and G. G. Qiao, *Chemical Science*, 2014, **5 (9)**, 3374–3380.
- 32 T. G. Pattison, A. Spanu, A. M. Friz, Q. Fu, R. D. Miller, and G. G. Qiao, ACS Applied Materials and Interfaces, 2020, 12 (3), 4041–4051.
- 33 T. G. Pattison, S. Wang, R. D. Miller, G. Liu, and G. G. Qiao, *Nat Commun*, 2022, **13 (1)**, 1941.
- 34 Z. Mossayebi, V. F. Jafari, P. A. Gurr, R. Simons, and G. G. Qiao, *ACS Applied Materials and Interfaces*, 2023, **15 (5)**, 7454–7465.
- 35 J. O. Zoppe, N. C. Ataman, P. Mocny, J. Wang, J. Moraes, and H.-A. Klok, *Chem. Rev.*, 2017, **117 (3)**, 1105–1318.
- 36 L. Grill, and S. Hecht, Nat. Chem., 2020, 12 (2), 115-130.
- 37 M. B. Dinger, and J. C. Mol, European Journal of Inorganic Chemistry, 2003, 2003 (15), 2827–2833.
- 38 M. B. Dinger, and J. C. Mol, *Organometallics*, 2003, **22 (5)**, 1089–1095.
- 39 X. Hong, Y. Gan, and Y. Wang, Surface & Interface Analysis, 2011, 43 (10), 1299–1303.
- 40 S. Li, Y. Hou, M. Kappl, W. Steffen, J. Liu, and H. Butt, *Advanced Materials*, 2022, **34 (34)**, 2203242.

- 41 X. Li, K. Zhang, Y. Zhao, K. Zhu, and X. Yuan, *Progress in Organic Coatings*, 2015, **89**, 150–159.
- 42 A. J. Meuler, J. D. Smith, K. K. Varanasi, J. M. Mabry, G. H. McKinley, and R. E. Cohen, *ACS Appl. Mater. Interfaces*, 2010, **2 (11)**, 3100–3110.
- 43 K. Kendall, J. Phys. D: Appl. Phys., 1971, 4 (8), 1186–1195.
- 44 C. Wang, M. C. Gupta, Y. H. Yeong, and K. J. Wynne, *J of Applied Polymer Sci*, 2018, **135 (24)**, 45734.
- 45 Yu. B. Chernyak, and A. I. Leonov, *Wear*, 1986, **108 (2)**, 105–138
- 46 J. Ji, N. Liu, Y. Tian, H. Zhai, S. Zhao, G. Liu, Y. Wei, and L. Feng, Chemical Engineering Journal, 2023, 474, 145537.
- 47 P. Irajizad, A. Al-Bayati, B. Eslami, T. Shafquat, M. Nazari, P. Jafari, V. Kashyap, A. Masoudi, D. Araya, and H. Ghasemi, *Mater. Horiz.*, 2019, **6 (4)**, 758–766.
- 48 M. S. Sanford, J. A. Love, and R. H. Grubbs, *Organometallics*, 2001, **20 (25)**, 5314–5318.
- 49 C. Acebo, X. Fernández-Francos, X. Ramis, and À. Serra, *Reactive and Functional Polymers*, 2016, **99**, 17–25.

Ultra-Low Ice Adhesion Enabled by Nano-Engineered Poly (ionic liquid)-Elastomeric Films: Leveraging Aqueous Lubrication and Elasticity

Zahra Mossayebi, ab Paul A. Gurr, Ranya Simons*b and Greg G. Qiao*a

Data availability

The data supporting this article have been included as part of the Supplementary Information.

^{a.} Department of Chemical Engineering, The University of Melbourne, Melbourne, Victoria 3010, Australia.

b. CSIRO manufacturing, Melbourne, Victoria 3196, Australia.